JOURNAL OF MATERIALS SCIENCE 37 (2002) 4473–4480

Microstructures and modification performance of melt-spun Al-10 Sr alloy

ZHONGHUA ZHANG, XIUFANG BIAN, YAN WANG, XIANGFA LIU
The Key Laboratory of Liquid Structure and Heredity of Materials, Ministry of Education, Shandong University, 73 Jingshi Road, Jinan 250061, People's Republic of China
E-mail: zh_zhang@sdu.edu.cn
E-mail: xfbian@sdu.edu.cn

The microstructures of Al-10 Sr alloy quenched at various wheel speeds have been investigated using X-ray diffractometry (XRD) and transmission electron microscopy (TEM). The experimental results show that the microstructures of melt-spun Al-10 Sr alloy are quite different from those of ingot-like alloy consisting of coarse plate-like Al_4Sr embedded in the eutectic matrix. For lower wheel speeds of 500 and 1000 rpm, the microstructure is composed of nanoscale particle-like Al_4Sr embedded in α-Al solid solution. With wheel speeds exceeding 1500 rpm, the formation of primary Al_4Sr phase is completely suppressed and the eutectic microstructure consisting of alternate dark and bright zones is obtained. Eutectic Al_4Sr in dark zones is stripe-like and irregular blocky, while regular stripe-like in bright zones, about 10–20 nm in width. Furthermore, modification tests indicate that the modification performance of melt-spun Al-10 Sr alloy is much better than that of ingot-like alloy, reducing the amount of Sr addition and greatly shortening the incubation time. The reasons for the formation of microstructures and the improvement of modification performance of melt-spun Al-10 Sr master alloy have also been discussed.

1. Introduction

Al-Sr alloys are widely used in industrial practice for the modification of Al-Si alloys by which the eutectic Si is converted from a coarse flake into a fine fibrous morphology [1–3]. The different microstructures of Al-Sr master alloys with the same composition have a significant effect on modification for Al-Si alloys. Compared to Al-Sr ingots, the deformed Al-Sr master alloys have obviously different modifying efficiency, namely, may decrease the strontium addition and reduce the incubation time thereafter [4].

Ever since the process of rapid quenching of metallic melts was first introduced by Duwez and his collaborators in 1960 [5], a great variety of techniques have been introduced to achieve rapid solidification of metals. And melt spinning process is the most commonly used method nowadays to produce long and continuous ribbons [6]. Rapid solidification processing (RSP) is capable of producing grain refinement and inducing one or more of the metastable effects, viz., extension of solid solubility limits and formation of metastable crystalline, quasicrystalline or glassy phases. A number of studies [7–10] have been undertaken to investigate the microstructures of rapidly solidified metals. However, few studies have been made on the microstructural characteristics and modification performance of rapidly solidified Al-Sr master alloys. Wiggen [11] has reported that the size of Al_4Sr compound is about $1 \times 4\ \mu m$ in the commercial Al-10 Sr rod prepared by gas atomization and subsequent extrusion. Very shorter incubation time is required for the atomized and extruded Al-10 Sr rod to modify Al-Si alloys. The addition amount of Al-Ti-Sr master alloy is reduced by rapid solidification technology, keeping the same degree of modification and refinement [12]. The present work serves to investigate the effect of cooling rate on the microstructures of melt-spun Al-10 Sr alloy prepared using pure elements. The modification performance of rapidly solidified Al-10 Sr alloy is also examined.

2. Experimental

Elemental Al (99.9% purity) and Sr (99.7% purity) were used to prepare alloys of nominal composition Al-10 Sr (wt%). The charges were melted in a graphite clay crucible using a medium frequency induction electric furnace under an inert argon atmosphere and were cast into ingots in copper chill mould. The actual composition of the alloy was determined to be 9.845 wt% Sr, using the atomic absorption method. The master alloy was remelted by high-frequency induction heating in quartz crucible in a controlled inert atmosphere. The melt was first heated to 1200°C, held at that temperature for 5 min, and then cast into continuous ribbons using the single roller melt spinning technique under a partial argon atmosphere. Different wheel speeds of 500, 1000, 1500, and 1800 revolutions per minute (rpm) were adopted to produce the ribbons different in thickness.

X-ray diffractometry (XRD) with Cu K_α radiation was used for phase identification in melt-spun Al-10 Sr alloy. The diffractometer was calibrated using a high purity silicon standard for accurate calculation of matrix lattice parameters. Higher order reflections were used in the lattice parameter calculations which were plotted against the Nelson-Riley function. The extrapolated plot gives the corrected matrix lattice parameter. Microstructural characterization of the ribbons was carried out using transmission electron microscopy (TEM). In addition, the foil specimens were punched directly from the melt-spun ribbons and were prepared by ion beam thinning.

The modification performance of both ingot-like and melt-spun Al-10 Sr master alloy was tested using different additions of Sr. The hypoeutectic Al-10 wt% Si alloy used in this work was prepared from commercial pure Al (99.7 wt%) and Si (99.5 wt%) using an electric resistance furnace in a graphite clay crucible. The Al-10 Sr master alloy was added into molten Al-10 Si alloy at about 730°C. Maintaining the temperature for a certain time, the molten alloy was poured into a permanent mould. The Sr-modified samples deeply etched in 0.1 wt% HF were examined using scanning electron microscopy (SEM). The evaluation of the modification rating was performed according to Ref. [13].

3. Results

3.1. Microstructures of melt-spun Al-10 Sr alloy quenched at various wheel speeds

Fig. 1 shows the XRD patterns of melt-spun Al-10 Sr alloy. The melt-spun alloy is identified to be composed of two phases: α-Al and Al_4Sr in terms of XRD patterns. It also can be seen from Fig. 1 that wheel speed has a marked effect on XRD patterns of melt-spun Al-10 Sr alloy. The height of the peaks of Al_4Sr phase becomes shorter and the width becomes broader with increasing wheel speed from 500 to 1800 rpm. The height and width of the diffraction peaks of α-Al matrix show a similar tendency. The widening of the diffraction peaks of both Al_4Sr phase and α-Al matrix indicates that the size of the two phases in Al-10 Sr decreases with increasing wheel speed.

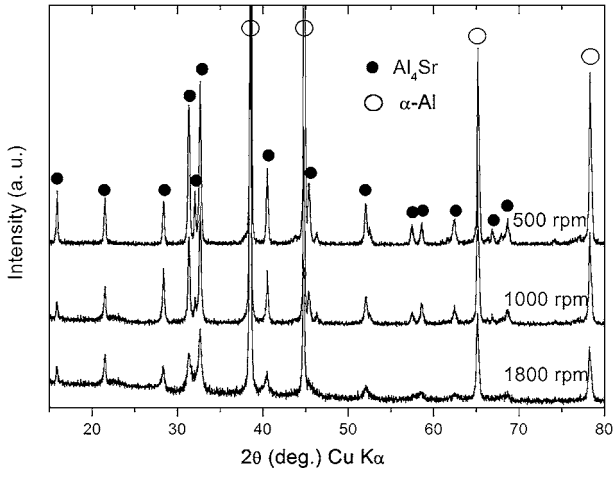

Figure 1 XRD patterns of melt-spun Al-10 Sr alloy.

TABLE I Variation of matrix lattice parameter with respect to wheel speed for Al-10 Sr alloy

Wheel speed (rpm)	500	1000	1800
Lattice parameter (nm)	0.40447	0.40464	0.40472

The lattice parameter of α-Al matrix was plotted against the Nelson-Riley function for the melt-spun Al-10 Sr alloy. The extrapolation of the plot to the ordinate gives the corrected value of the matrix lattice parameter. The calculated matrix lattice parameters are slightly less than that of pure Al (0.40495 nm). Furthermore, the matrix lattice parameter increases with increasing wheel speed, seen in Table I. The following two respects should be taken into consideration for the variation of matrix lattice parameter. The atomic radius of Sr (0.215 nm) is much bigger than that of Al (0.143 nm), which may result in the increase of lattice parameter of α-Al with Sr in solid solution. The bonding strength of Al-Sr is greater than Al-Al, which may give rise to the shrinkage of matrix. Moreover, the latter may be the dominating factor. Therefore, Sr in solid solution in melt-spun Al-10 Sr alloy leads to the decrease of matrix lattice parameter. However, the solid solubility of Sr in α-Al matrix increases with increasing wheel speed and the atomic size effect may become more important. Thus, the matrix lattice parameter increases with increasing wheel speed, but still less than that of pure Al.

Fig. 2 shows the microstructure of ingot-like Al-10 Sr alloy deeply etched. The microstructure is composed of primary Al_4Sr phase and the eutectic (α-Al + Al_4Sr). The α-Al matrix was removed to show the three-dimensional morphologies of primary and eutectic Al_4Sr. The primary Al_4Sr is coarse plate-like, about 150–300 μm in length and 15–20 μm in thickness. The eutectic Al_4Sr is very thin and continuous flakes.

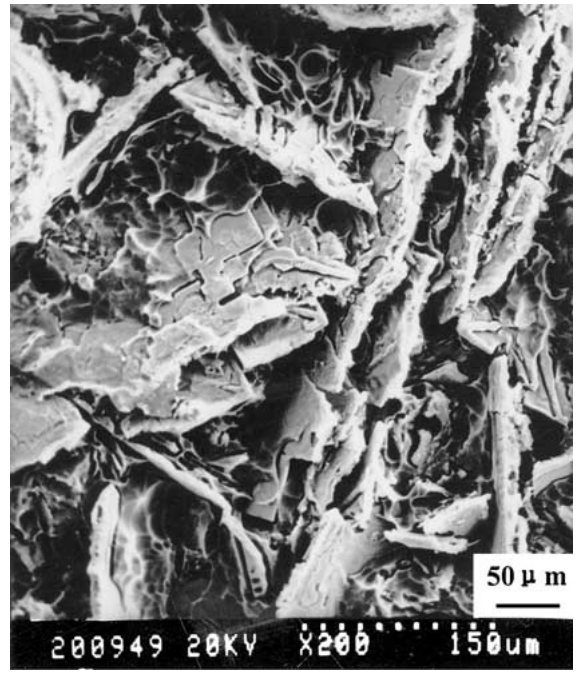

Figure 2 SEM image showing the microstructure of ingot-like Al-10 Sr alloy deeply etched by 1% NaOH aqueous solution.

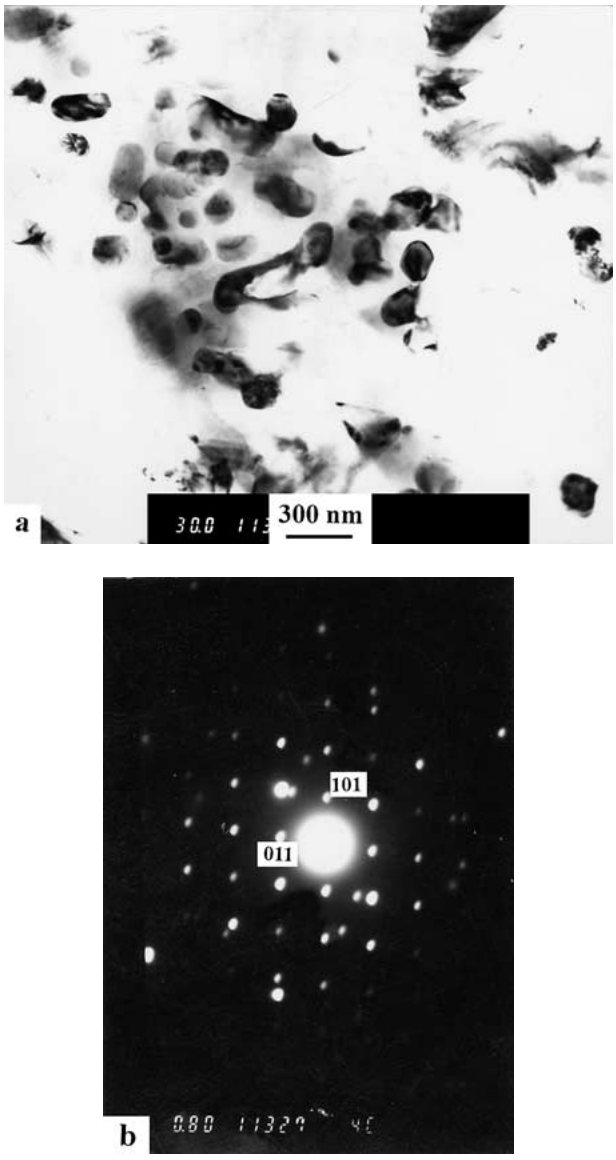

Figure 3 TEM bight-field image of melt-spun Al-10 Sr alloy quenched at the wheel speed of 500 rpm. (a) and SAED pattern of Al_4Sr [$\bar{1}\bar{1}1$] zone axis (b).

Fig. 3a shows the TEM bright-field image of melt-spun Al-10 Sr alloy quenched at the wheel speed of 500 rpm. Fig. 3b is the [$\bar{1}\bar{1}1$] zone axis (ZA) SAED pattern of Al_4Sr phase. The primary Al_4Sr particles are embedded in α-Al matrix and no eutectic Al_4Sr phase is observed, which is quite different from the microstructure of non-RSP ingot-like Al-10 Sr alloy shown in Fig. 2. The size of Al_4Sr particles ranges from 100 to 400 nm. The morphologies of Al_4Sr phase are diverse, including rounded, elliptic, angular, near-rectangular and other irregular particles.

Fig. 4 shows the TEM bright-field images (a, b) and corresponding SAED patterns (c, d) of melt-spun Al-10 Sr alloy quenched at the wheel speed of 1000 rpm. SAED patterns indicate that the microstructure is still composed of two phases: α-Al matrix and Al_4Sr particles, similar to the alloy quenched at the wheel speed of 500 rpm. The size of the Al_4Sr particles is about 200 nm, but some particles are very small, only 20–50 nm in size, shown in Fig. 4a. Furthermore, most of the particles are rounded or near-rounded. On the whole, the size of the Al_4Sr particles becomes smaller and the morphology becomes regular with increasing wheel speed from 500 to 1000 rpm. A great number of Al_4Sr particles, about 20–50 nm in size, are embedded in α-Al matrix, as seen in Fig. 4b. And a small amount of eutectic Al_4Sr is observed, as indicated by an arrow in Fig. 4b. The SAED pattern from Fig. 4a consists of two sets of Bragg reflections: the strong reflections from α-Al [013] zone axis and the weak ones from Al_4Sr [$\bar{1}$20] zone axis, as shown in Fig. 4c. It is obvious that the orientation relationship α-Al [013]$\|Al_4Sr$ [$\bar{1}$20] has been determined. Moreover, the (200) crystal face of α-Al is parallel to the (002) crystal face of Al_4Sr. Because of the very small Al_4Sr particles (Fig. 4b), the SAED pattern exhibits polycrystalline diffraction rings, corresponding to (103), (210) and (206) crystal faces of Al_4Sr respectively, as illustrated in Fig. 4d. The strong reflections are the [136] ZA SAED pattern of α-Al.

Quite different from ingot-like and Al-10 Sr alloy quenched at the slower wheel speed (500 and 1000 rpm), the microstructure of melt-spun Al-10 Sr alloy quenched at the wheel speed of 1500 rpm is shown in Fig. 5. As shown in Fig. 5a, the microstructure of the alloy ribbons consists of two alternate zones: bright zones and dark zones, respectively. To clearly illustrate the microstructural characteristic of both bright and dark zones, the enlarged TEM images are shown in Fig. 5b and c, respectively. From the enlarged images, it can be seen that both the two zones are on the whole similar and are composed of ultrafine bright and dark stripes. It is interesting that the primary Al_4Sr phase disappears and the alternate bright and dark stripes form the complete eutectics in Al-10 Sr alloy quenched at higher wheel speed (1500 rpm). The morphologies of the Al_4Sr phase in dark zones are diverse, including stripes and irregular blocks. However, the microstructure of bright zones is homogeneous and all the Al_4Sr phase is stripe-like. The size of the Al_4Sr phase in bright zones is about 10 nm in width. As shown in Fig. 5d, the SAED pattern from Fig. 5b includes two sets of Bragg reflections: the strong reflections from α-Al [100] zone axis and the weak ones from Al_4Sr [001] zone axis, which demonstrates the typical eutectic characteristic of melt-spun Al-10 Sr alloy. Apparently, there exists the orientation relationship α-Al [100]$\|Al_4Sr$ [001]. Furthermore, the (020) and (022) crystal faces of α-Al are parallel to the (200) and (110) crystal faces of Al_4Sr, respectively.

The microstructure of the Al-10 Sr ribbons quenched at further higher wheel speed of 1800 rpm is similar to that quenched at 1500 rpm, shown in Fig. 6. As shown in Fig. 6a, the microstructure of the alloy also consists of alternate dark and bright zones, which are both eutectic. Fig. 6b shows the corresponding SAED pattern which also includes two sets of Bragg reflections, [100] ZA α-Al (strong reflections)$\|$[001] ZA Al_4Sr (weak reflections), similar to that shown in Fig. 5d.

3.2. Modification performance of melt-spun Al-10 Sr alloy ribbons

Fig. 7 shows the variation of modification rating of Al-10 wt% Si with the amount of Sr addition in the form of ribbons and ingots. The modification rating reaches

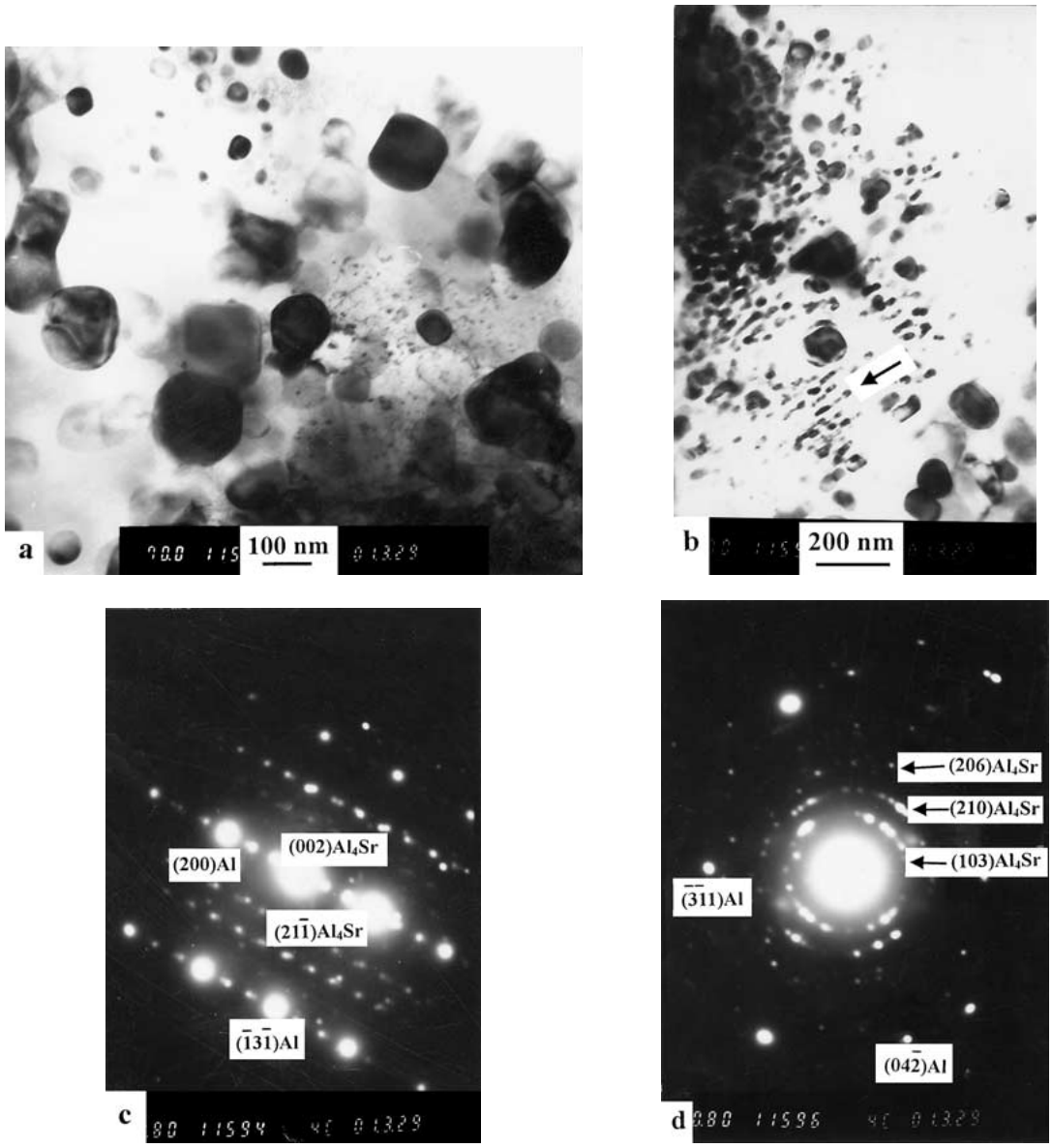

Figure 4 TEM bright-field images (a, b) and corresponding SAED patterns (c, d) of melt-spun Al-10 Sr alloy quenched at the wheel speed of 1000 rpm.

5 with 0.05 wt% Sr addition in the form of ingots, but only 0.03 wt% Sr addition in the form of melt-spun ribbons. Under the same modification condition, the amount of Sr addition in the form of ribbons could be reduced by 40%, compared with that in the form of ingots. The variation of modification rating with holding time after Sr addition is shown in Fig. 8. Holding about 20 min after Sr addition in the form of ingots, the modification rating reaches 5. For Al-Sr alloy ribbons, however, the holding time could be greatly reduced obtaining the optimum modification effect (modification rating 5). In other words, the "zero" incubation time could be realized when the melt-spun Al-Sr ribbons were used. Fig. 9 shows the three-dimensional morphologies of eutectic Si in Sr-modified Al-10 wt% Si alloy deeply etched in 0.1 wt% HF aqueous solution. The α-Al matrix was removed to show clearly the morphologies of eutectic Si. For the Al-10 wt% Si alloy modified by Al-10 Sr ribbons, the fibrous branches of eutectic Si are very long and fine, as seen in Fig. 9a. On the contrary, the branches are shorter and coarser for the alloy modified by ingot-like Al-10 Sr, as seen in Fig. 9b.

4. Discussion

4.1. Effect of cooling rate on the microstructures of Al-10 Sr alloy

According to binary Al-Sr phase diagram [14], a eutectic occurs at about 2.4 wt% Sr and 654°C in high aluminum alloys. Therefore, Al-10 Sr alloy is hypereutectic and the microstructure of Al-10 Sr alloy is composed of primary Al_4Sr phase embedded in the α-Al/Al_4Sr eutectic matrix under normal solidification conditions, as shown in Fig. 2. The primary Al_4Sr phase is plate-like, about 150–300 μm in length and 15–20 μm in thickness. The ingot-like Al-10 Sr alloy is very brittle. Rapid solidification has a significant effect on microstructures of Al-10 Sr alloy. The microstructures of melt-spun Al-10 Sr alloy are quite different from those of the alloy solidified under conventional casting conditions. For the Al-10 Sr alloy quenched at the wheel speeds of 500 and 1000 rpm, the primary Al_4Sr phase is very fine particles, less than 400 nm in size, embedded in α-Al solid solution. The alloy ribbons quenched at these speeds are ductile, which allows for the subsequent extrusion after rapid solidification.

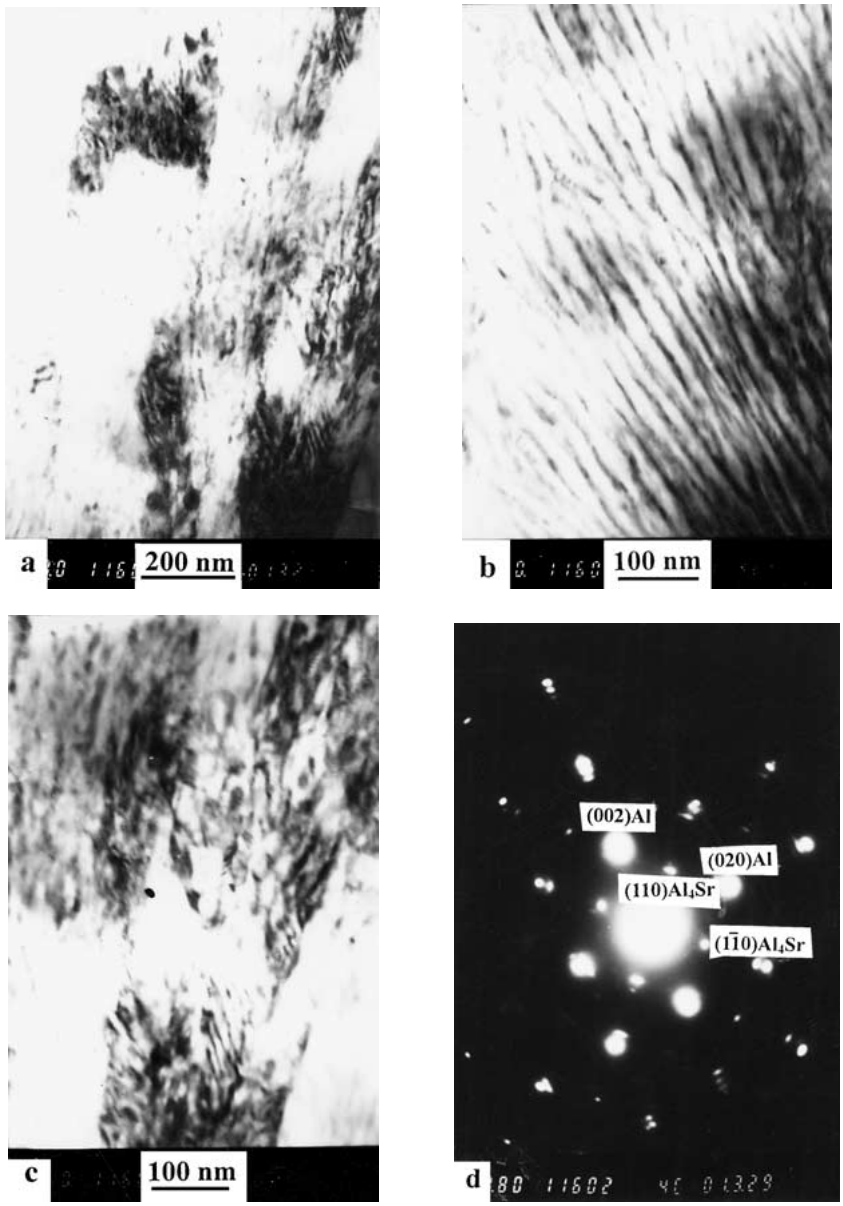

Figure 5 TEM bright-field image showing the microstructure of melt-spun Al-10 Sr alloy quenched at the wheel speed of 1500 rpm (a); enlarged images corresponding to bright zones (b) and dark zones (c), respectively; and the SAED pattern (d).

Nevertheless, the primary Al_4Sr phase disappears and the alloy exhibits complete eutectic microstructure composed of two alternate dark and bright zones, for the alloy quenched at wheel speeds exceeding 1500 rpm. And the alloy ribbons quenched at higher speeds become a little brittle. The ductility (or brittleness) of the Al-10 Sr alloy is presented in Table II. Here, the ductility/brittleness description is only qualitative observation for melt-spun ribbons due to the difficulties in measurement.

The cooling rate plays a key role in the formation of the rapidly solidified microstructures mentioned above. The cooling rate R was roughly estimated from the equation [15]

TABLE II Ductility (or brittleness) of the Al-10 Sr alloy

		Ribbons quenched at			
Conditions	Ingots	500 rpm	1000 rpm	1500 rpm	1800 rpm
Ductile/Brittle	Very brittle	Ductile	Ductile	Brittle	Brittle

$$R = h(T_1 - T_0)/C_P \rho t \tag{1}$$

where h is the heat transfer coefficient between the ejected molten alloy and the rotating substrate, T_1 and T_0 are the molten and the substrate temperature, respectively, ρ the density and C_p the specific heat of the alloy, and t the thickness of the solidified ribbon specimen. In this work, a value of 1.0 cal $\cdot$ (cm^2 K s)$^{-1}$ was assigned to h for the copper roller [16]. The specific heat of the alloy at room temperature was determined to be 0.78774 J $\cdot$ g^{-1} $\cdot$ K^{-1} using DSC. The density of the alloy, ρ, may be estimated, as a first approximation, by

$$\rho = \sum X_i \cdot \rho_i \tag{2}$$

where X_i represents the mole fraction of component i in the alloy, and ρ_i is the density of the pure component i. The density of Al-10 Sr alloy is determined to be 2.697 g $\cdot$ cm^{-3}. The calculated cooling rates are presented in Table III.

TABLE III Ribbon thickness and cooling rate of melt-spun Al-10 Sr alloy

Wheel speed (rpm)	500	1000	1500	1800
Thickness (μm)	70	50	30	25
Cooling rate (K s^{-1})	3.3×10^5	4.6×10^5	7.7×10^5	9.3×10^5

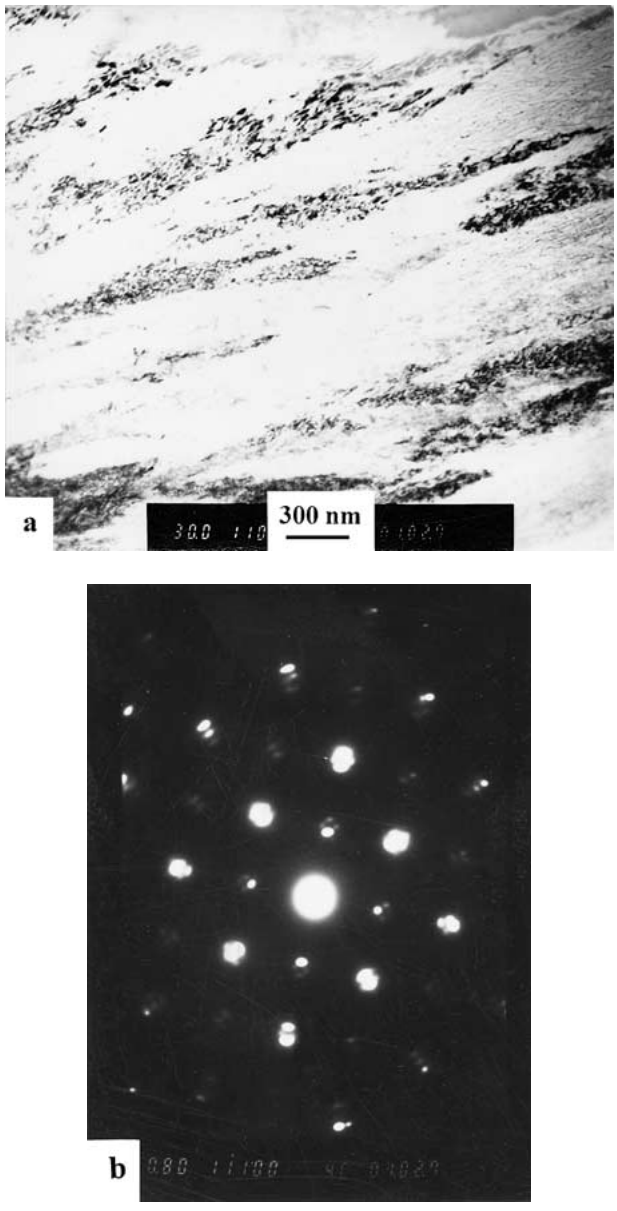

Figure 6 TEM bright-field image (a) and SAED pattern (b) of melt-spun Al-10 Sr alloy quenched at the wheel speed of 1800 rpm.

For the Al-10 Sr alloy solidified under conventional casting conditions ($R < 10^3$ K s^{-1}), the degree of undercooling is very small, the primary Al_4Sr phase is first formed from the melt, and then the eutectic reaction takes place when the temperature is depressed below eutectic temperature. The primary temperature range (ΔT) is defined as follows:

$$\Delta T = T_L - T_E \quad (3)$$

Where T_L is the temperature of the liquidus and T_E is the eutectic temperature. The primary temperature

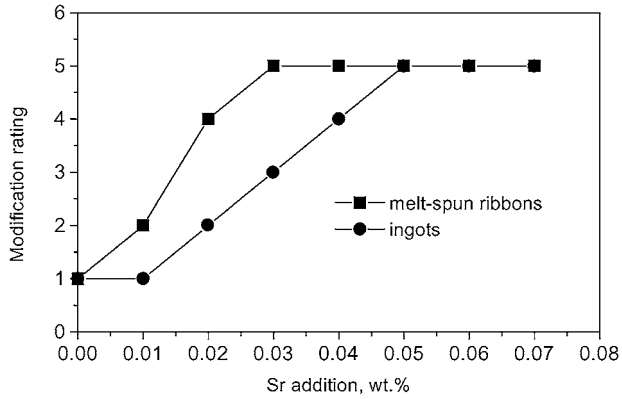

Figure 7 Sr addition vs. modification rating in the permanent mould.

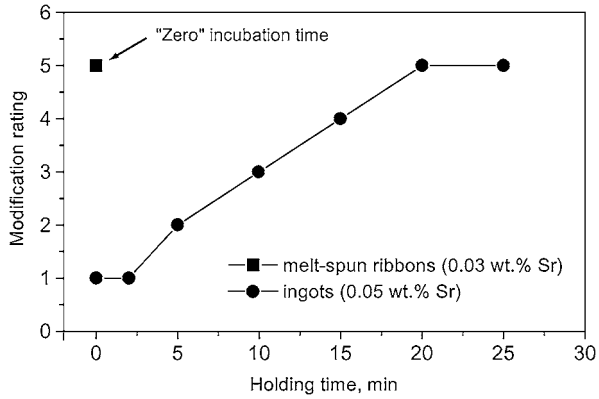

Figure 8 Holding time vs. modification rating in the permanent mould.

range is great enough for primary Al_4Sr phases to grow into coarse plate-like. However, the melt-spun Al-10 Sr alloy is another case. The most commonly used methods for generating high liquid undercoolings prior to solidification involve a rapid quenching from the melt. Indeed, the main attention in RSP methods has been focused upon the attainment of high cooling rates in the range of 10^4–10^8 K s^{-1} [17]. In our work, melt spinning technique with various wheel speeds is adopted to produce different cooling rates, as seen in Table III. Fig. 10 shows the Al-rich section of Al-Sr phase diagram. For the Al-10 Sr alloy quenched at wheel speed of 500 rpm, the melt is undercooled and ΔT markedly decreases, compared to that solidified under common conditions. The primary Al_4Sr phase may still form in the melt, but the growth of primary Al_4Sr phase is suppressed, therefore, the size of primary Al_4Sr phase is very small (20–400 nm) and the morphology is particle-like because the growth time is too short to allow well-developed faceted crystals to develop. Because of the high level of undercooling, the solid-liquid interface of the remaining melt moves at a velocity sufficient to suppress solute partitioning through the process of solute trapping at the interface, and the eutectic reaction is also suppressed. The microstructure comprises particle-like Al_4Sr phase embedded in α-Al matrix. With wheel speed increasing to 1000 rpm, the undercooling increases and ΔT further decreases. The size of primary Al_4Sr phase becomes smaller, less than 200 nm. The morphology becomes rounded or near-rounded. Furthermore, the eutectic microstructure is observed in the

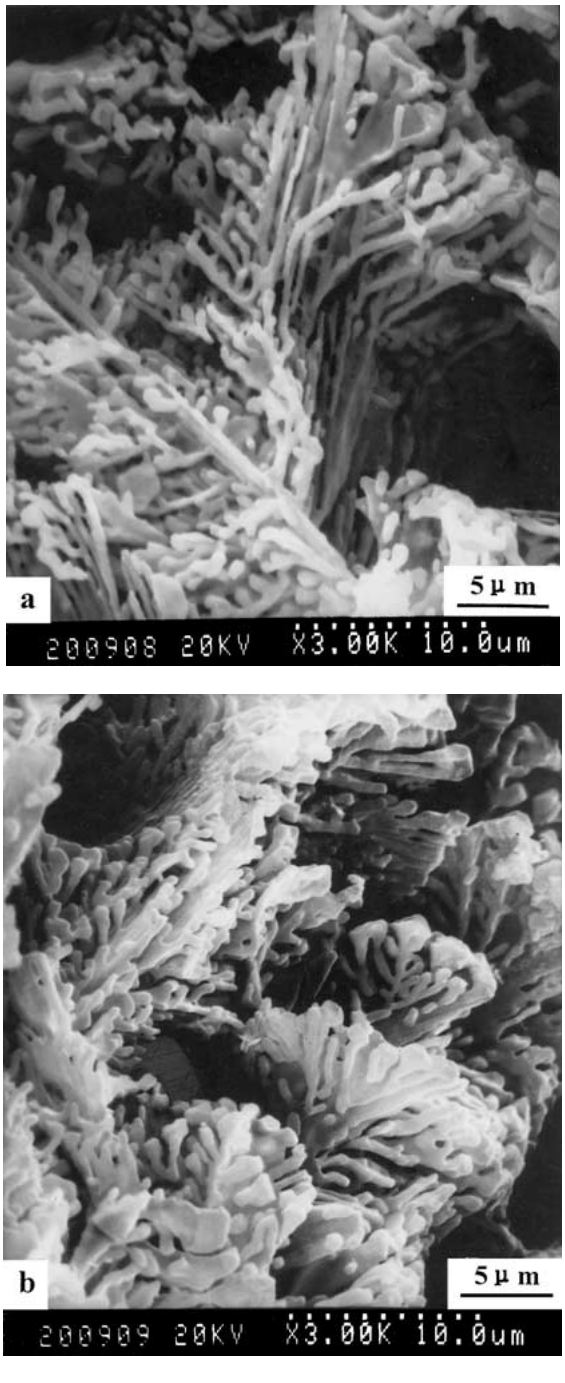

Figure 9 SEM images showing the morphologies of eutectic Si in Sr-modified Al-10 wt% Si alloy deeply etched in 0.1 wt% HF aqueous solution. ((a) addition of 0.03 wt% Sr in the form of ribbons; (b) addition of 0.05 wt% Sr in the form of ingots).

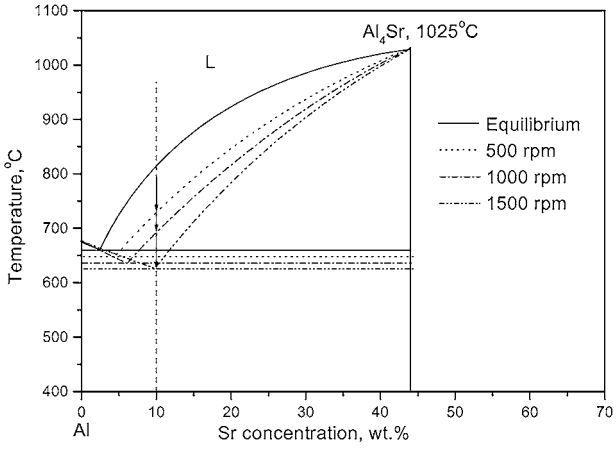

Figure 10 Al-rich section of Al-Sr phase diagram.

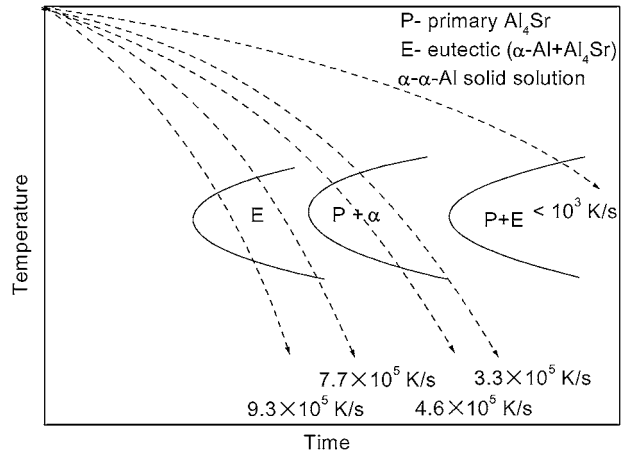

Figure 11 Schematic temperature-time-transformation diagram of Al-10 Sr alloy.

local part of the alloy. With wheel speeds exceeding 1500 rpm, the undercooling of the melt is great enough to completely suppress the formation of the primary Al_4Sr phase and the eutectic microstructure composed of alternate stripe-like Al_4Sr and α-Al is obtained. The microstructures of Al-10 Sr alloy exhibit coarse plate-like Al_4Sr phase embedded in the eutectic (P + E), then very small particle-like Al_4Sr embedded in the α-Al solid solution (P + α), and finally the complete eutectic (E) with increasing cooling rate from less than 10^3K s^{-1} to about 10^6 K s^{-1}, as schematically illustrated in Fig. 11. Therefore, the critical cooling rate at which the formation of primary Al_4Sr is completely suppressed and the eutectic is obtained is estimated to be between 4.6×10^5(1000 rpm) and 7.7×10^5 K s^{-1} (1500 rpm).

4.2. Effect of RSP on the modification performance of Al-10 Sr alloy

Based on the results previously mentioned, the modification performance of melt-spun Al-10 Sr alloy is much better than that of the ingot-like alloy. The amount of Sr addition can be reduced by 40% through rapid solidification technology, keeping the same degree of modification effect. In general, the melt after Sr addition in the form of ingots should be held about 15–20 min at a certain temperature before pouring. However, the incubation time (the minimum time needed to reach the optimum modification effect after Sr addition) is greatly reduced to almost zero through addition of melt-spun Al-10 Sr ribbons. Moreover, the branches of eutectic Si in the Al-10 wt% Si alloy modified by melt-spun Al-10 Sr ribbons are longer and thinner than those by ingot-like master alloy, seen in Fig. 9. The industrial application of rapidly solidified Al-Sr alloys is promising to reduce the cost and raise productivity.

The reasons for the improvement of modification performance of melt-spun Al-10 Sr master alloy can be speculated as follows:

The very fine microstructures of the master alloy. The Al-Sr master alloy is added into the Al-Si melt, elemental Sr is decomposed from Al_4Sr and then plays an important role in subsequent solidification process. The

remarkable morphological feature on the modification is reported to be an abnormal increase in twinning of eutectic Si which results in instability of interfacial area and permits repeated branching of the Si phase [18, 19]. The primary Al_4Sr phase in ingot-like Al-10 Sr is very coarse, about 150–300 μm in length and 15–20 μm in thickness. When the ingot master alloy is added into the Al-Si melt, the dissociation of elemental Sr from Al_4Sr needs more time. After the Al-Sr ribbons are put into the Al-Si melt, however, Sr can rapidly dissociate from Al_4Sr because of the very fine Al_4Sr phase (10– 400 nm). Furthermore, the Al-Sr melt is quenched at very high cooling rates (greater than 10^5 K s^{-1}) and the metastable microstructures are obtained. In addition, the defects such as grain boundaries and dislocations increase, which also leads to the increase of dissolution rate of Al_4Sr. Therefore, the incubation time can be greatly reduced. The loss of Sr is then reduced and the recovery factor is very high, which partially contributes to the improvement of modification effect of melt-spun Al-10 Sr alloy. However, the Al-10 Sr alloy quenched at various wheel speeds possesses almost the same modification performance because the size of Al_4Sr phase is on the same order of magnitude.

5. Conclusions

1. The microstructures of the Al-10 Sr alloy quenched at lower wheel speeds of 500 and 1000 rpm are composed of particle-like Al_4Sr embedded in α-Al solid solution ($P + \alpha$), compared to the ingot-like alloy which comprises primary plate-like Al_4Sr embedded in the α-Al/Al_4Sr eutectic ($P + E$). The size of Al_4Sr phase in the melt-spun ribbons ranges from 20 to 400 nm, much smaller than that of ingots, about 150–300 μm in length and 15–20 μm in thickness.

2. With wheel speed exceeding 1500 rpm, the formation of primary Al_4Sr phase is completely suppressed owing to the high-level undercooling and the eutectic microstructure consisting of alternate dark and bright zones is obtained. Both bright zones and dark zones are completely eutectic and similar in composition. The critical cooling rate at which the formation of primary Al_4Sr is completely suppressed and the eutectic is obtained is estimated to be between 4.6×10^5 (1000 rpm) and 7.7×10^5 K s^{-1} (1500 rpm).

3. The modification performance of melt-spun Al-10 Sr alloy is much better than that of ingot-like alloy. The amount of Sr addition can be reduced by 40% through rapid solidification technology, keeping the same degree of modification effect. In particular, the incubation time after Sr addition is reduced to almost zero. Moreover, the branches of the eutectic Si in the alloy modified by ribbons are much finer and longer than those modified by ingot. The beneficial effect of the melt-spun alloy on modification may be due to the much finer and more defective microstructures compared to the ingot-like alloy. The Al-10 Sr alloy quenched at various wheel speeds possesses the same modification performance, despite different microstructures.

Acknowledgements

The authors give grateful thanks for the support of the National Natural Science Foundation of China (Grant No. 50071028) and Shandong Natural Science Foundation of China (Grant No. Z2001F02).

References

1. J. Y. CHANG and H. S. KO, *J. Mater. Sci. Lett.* **19** (2000) 197.
2. B. HESHMATPOUR, in "Light Metals," edited by R. Huglen (TMS, Warrendale, 1997) p. 801.
3. D. EMADI, J. E. GRUZLESKI and J. M. TOGURI, *Metall. Trans.* B **24** (1993) 1055.
4. J. Y. QIN, X. F. BIAN, X. J. HAN, X. F. LIU and J. J. MA, *Chinese J. Mater. Res.* **13**(2) (1999) 162.
5. P. DUWEZ, R. H. WILLENS and W. KLEMENT, *J. Appl. Phys.* **31** (1960) 1136, 1500; also *Nature* **187** (1960) 869.
6. T. R. ANANTHARAMAN and C. SURYANARAYANA, in "Rapidly Solidified Metals" (Trans Tech Publications, Aedermannsdorf, Switzerland, 1987).
7. M. G. CHU, *Mater. Sci. Eng.* A **179/180** (1994) 669.
8. T. GROSDIDIER, P. KERAMIDAS, G. SHAO and P. TSAKIROPOULOS, *ibid.* A **267** (1999) 60.
9. T. GROSDIDIER, P. KERAMIDAS, J. J. FUNDENBERGER, F. WAGNER and P. TSAKIROPOULOS, *ibid.* A **267** (1999) 71.
10. D. H. PING, K. HONO and A. INOUE, *Metall. Mater. Trans.* A **31** (2000) 607.
11. P. C. VAN WIGGEN, in "Light Metals," edited by U. Mannweiler (TMS, Warrendale, 1994) p. 1057.
12. X. F. BIAN, X. H. LIN and X. F. LIU, *J. Mater. Sci.* **33** (1998) 99.
13. D. APELIAN, G. K. SIGWORTH and K. R. WHALER, *AFS Trans.* **92** (1984) 297.
14. B. CLOSSET, H. DUGAS, M. PEKGULERYUZ and J. E. GRUZLESKI, *Metall. Trans.* A **17** (1986) 1250.
15. H. JONES, in "Ultrarapid Quenching of Liquid Alloys, Treatise on Materials Science and Technology," Vol. 20, edited by H. Herman (Academic, New York, 1981) p. 29.
16. M. N. BURDEN and H. JONES, *J. Inst. Met.* **98** (1970) 249.
17. J. H. PEREPEZKO, *Mater. Sci. Eng.* A **179/180** (1994) 52.
18. J. M. DOWLING, J. M. CORBETT and H. W. KERR, *J. Mater. Sci.* **22** (1987) 4504.
19. S. Z. LU and A. HELLAWELL, *Metall. Trans.* A **18** (1987) 1721.

Received 11 July 2001
and accepted 27 March 2002